NASA TECHNICAL NOTE

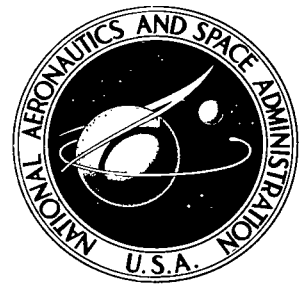

NASA TN D-6840
c. 1

NASA TN D-6840

OPTICAL ABSORPTION IN FUSED SILICA AT ELEVATED TEMPERATURES DURING 1.5-MeV ELECTRON IRRADIATION

by Albert B. Smith

Lewis Research Center
Cleveland, Ohio 44135

NATIONAL AERONAUTICS AND SPACE ADMINISTRATION • WASHINGTON, D. C. • JUNE 1972

1. Report No.	2. Government Accession No.	3. Recipient's Catalog No.
NASA TN D-6840		

4. Title and Subtitle	5. Report Date
OPTICAL ABSORPTION IN FUSED SILICA AT ELEVATED TEMPERATURES DURING 1.5-MeV ELECTRON IRRADIATION	June 1972
	6. Performing Organization Code
7. Author(s)	8. Performing Organization Report No.
Albert B. Smith	E-6595
	10. Work Unit No.
9. Performing Organization Name and Address	112-02
Lewis Research Center National Aeronautics and Space Administration Cleveland, Ohio 44135	11. Contract or Grant No.
	13. Type of Report and Period Covered
12. Sponsoring Agency Name and Address	Technical Note
National Aeronautics and Space Administration Washington, D.C. 20546	14. Sponsoring Agency Code

15. Supplementary Notes

16. Abstract

An experimental determination of the optical transmission of Corning 7940 UV and Suprasil I and II fused silica has been made during 1.5-MeV electron bombardment. The fused silica reached temperatures ranging from 150° to 1000° C. The Lewis Research Center dynamitron provided electron current densities which corresponded to a dose rate of 2.6 to 20 Mrad/sec. The irradiation induced absorption was measured at 215.0, 270.0, and 450.0 nm (2150, 2700, 4500 Å). The length of each irradiation was sufficient so that an equilibrium between radiation induced coloration and high temperature annealing was reached. The experimental results indicate a significant optical absorption, with values of the induced absorption coefficient at 215.0 nm (2150 Å) of 14.5 to 2.2 cm^{-1}, at 270.0 nm (2700 Å) of 9.7 to 3.0 cm^{-1} and at 450.0 nm (4500 Å) of 3.7 to 0.5 cm^{-1}. This would make the use of fused silica as the separating wall material in the nuclear light bulb propulsion concept questionable.

17. Key Words (Suggested by Author(s))		18. Distribution Statement
Solid state	Glasses	Unclassified - unlimited
Radiation damage	Optical absorption	
Reactor technology	Fused silica	
Electron radiation	Optical transmission	

19. Security Classif. (of this report)	20. Security Classif. (of this page)	21. No. of Pages	22. Price*
Unclassified	Unclassified	36	$3.00

* For sale by the National Technical Information Service, Springfield, Virginia 22151

OPTICAL ABSORPTION IN FUSED SILICA AT ELEVATED TEMPERATURES DURING 1.5-MeV ELECTRON IRRADIATION

by Albert B. Smith

Lewis Research Center

SUMMARY

An experimental investigation was conducted to measure the level of irradiation-induced optical absorption existing in Corning 7940 UV and Suprasil I and II fused silica during 1.5-MeV electron bombardment. The Lewis Research Center dynamitron provided the electron beam at current densities which corresponded to a dose rate of 2.6 to 20 megarads per second. This is equivalent to the ionizing dose rate of a full-scale proposed operating nuclear light bulb engine. The electron beam heated the fused silica to temperatures ranging from 150° to 1000° C. Irradiation times of 1000 seconds or more were sufficient to permit an equilibrium between radiation induced coloration and thermal annealing of coloration by exposure to elevated temperature to be attained. Optical absorption was measured at the wavelength of 215.0 nanometers (2150 Å) which is the center of the irradiation-induced absorption band in fused silica, and at the additional wavelengths of 270.0 and 450.0 nanometers (2700 and 4500 Å). The optical transmission and specimen temperature were continuously recorded so that both steady-state and transient data were obtained.

The experimental results indicate at these wavelengths that the irradiation-induced absorption coefficient was an increasing function of the dose rate. Equilibrium values of the induced absorption coefficient at 215.0 nanometers (2150 Å) range from 14.5 to 2.2 centimeters^{-1}; at 270.0 nanometers (2700 Å) the values were 9.7 to 3.0 centimeters^{-1}; and at 450.0 nanometers (4500 Å) this range was 3.7 to 0.5 centimeters^{-1}. Specimens of 3.00 and 1.5-millimeter thickness were investigated and showed very similar results. No significant difference was noted between Suprasil I and Corning 7940 UV. The results of soft mounting the specimen using a ceramic gasket material or firm mounting of the specimen were essentially the same indicating there was no anomaly due to specimen stress at these elevated temperatures.

Since these experimental results indicate a significant optical absorption, particularly at the shorter wavelength, the use of fused silica as the separating wall material in the nuclear light bulb engine propulsion concept is questionable.

INTRODUCTION

One interesting nuclear propulsion concept is the gaseous core nuclear reactor. In one design fused silica is proposed as a transparent wall separating the fuel and the propellant. This nuclear light bulb (NLB) transfers the energy of the fissioning fuel by thermal radiation through the fused silica to a hydrogen propellant seeded with opaque particles. The radiant energy absorbed lies in the range of 200.0 to 1000.0 nanometers (2000 to 10 000 Å). Practical realization of this propulsion scheme depends in large measure upon the transparency of these cooled fused silica walls at these wavelengths, since the energy must radiate through them and increased absorption could heat the fused silica sufficiently to melt it.

During reactor operation, a large flux of a variety of nuclear radiations emanate from the fissioning fuel. These radiations will produce color centers in the fused silica walls surrounding the fuel. In the applications considered, the walls will be in the temperature range of 600° to 1000° C while the engine is operating. At such temperatures, the color centers tend to bleach out or be annihilated. Therefore, the optical transmission of the walls will be affected by two competing processes during steady-state operation of the engine: (1) the production of color centers tending to reduce the transmissivity and, (2) the annealing of these centers tending to restore the optical transmission.

Since a sufficient reduction in transmissivity will cause a structural failure in the wall material, in order for the NLB engine concept to be workable, it is necessary that the transparency be maintained at a high level throughout the entire operation of the engine. The prime objective of this experiment is the measurement of the irradiation induced absorption of likely candidates for wall materials under conditions closely simulating those of full-scale operating NLB engines.

The materials tested were samples of Corning 7940 UV and Suprasil (Amersil, Inc.). These samples were chosen because of their high purity, structural integrity, resistance to radiation damage, and transparency over a wide range of wavelengths and thermal conditions. The studies included fused silica of 1.5 and 3.0 millimeters thickness. For these materials, the most prominent radiation induced absorption band occurs at 215.0 nanometers (2150 Å) and there is a subsidiary peak at 270.0 nanometers (2700 Å). Measurements were made at these wavelengths as well as at 450.0 nanometers (4500 Å) in order to determine the width of the absorption band and to check absorption where strong absorption bands are not expected to exist. A dual beam recording spectrophotometer was designed and used for the optical transmission measurements.

A full-scale NLB engine can be expected to subject its walls to as much as 10 megarads per second dose rate for periods up to 1000 seconds at temperatures of 600° to 1000° C. The Lewis Research Center dynamitron provided 1.5-MeV electrons at current densities of 20 to 150 microamperes per square centimeter for times near

1000 seconds. This corresponds to an ionizing dose rate of 2.6 to 20 megarads per second for the required time period. Specimen temperature was governed by electron beam heating; irradiations at 80 to 150 microamperes per square centimeter heated the specimens to the temperature range of interest (600^{o} to 900^{o} C).

EXPERIMENTAL PROCEDURE AND APPARATUS

The various independent parts in the test section of the ratio recording spectrometer are shown in their overall relation to each other in two photographs. Figure 1 is a clear view from directly above the optical base. It shows the dynamitron electron beam transport tube attached to the sample box, as well as the mirrors, xenon lamp, rotating mirror, and the furnace on the reference optical path. A lower viewing angle looking down the length of the optical base is displayed in figure 2 giving the relation between the light source, the optical paths, and the monochromator. A block diagram of the optical setup is depicted in figure 3.

During a test run, the entire optical system was located in the immediate vicinity of the electron beam. It was thereby subjected to the large radiation field of the accelerator making it necessary to separate the electronic readout from the beam room. These controls were placed about 30 meters away in the dynamitron control room.

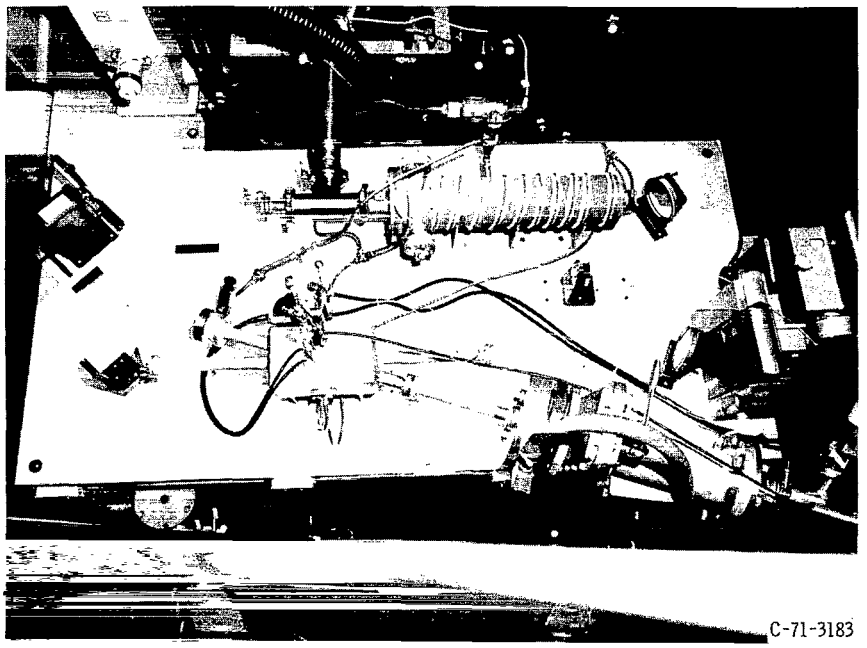

Figure 1. - Dual beam spectrometer (top view).

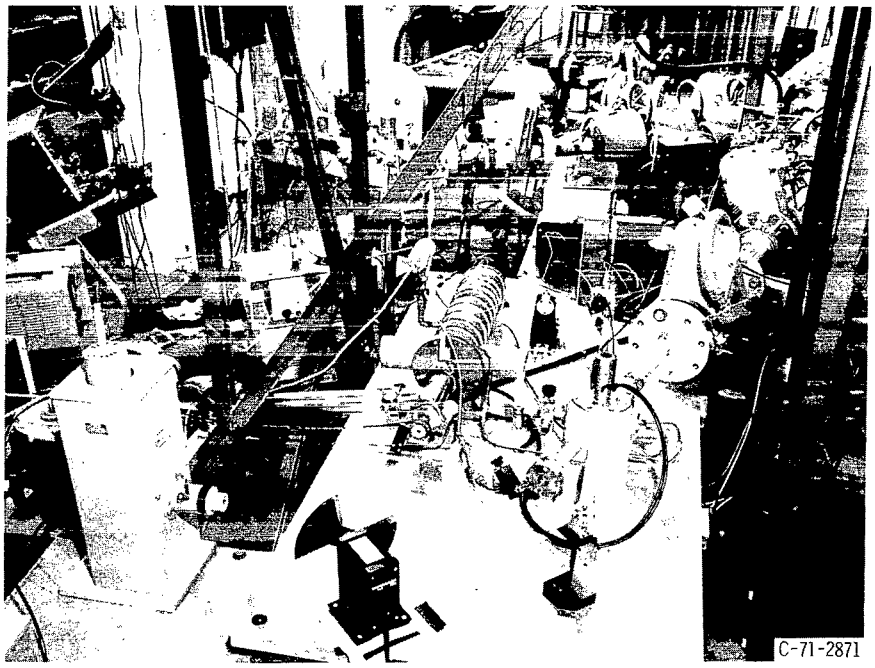

Figure 2. - Light source and dual beam spectrometer.

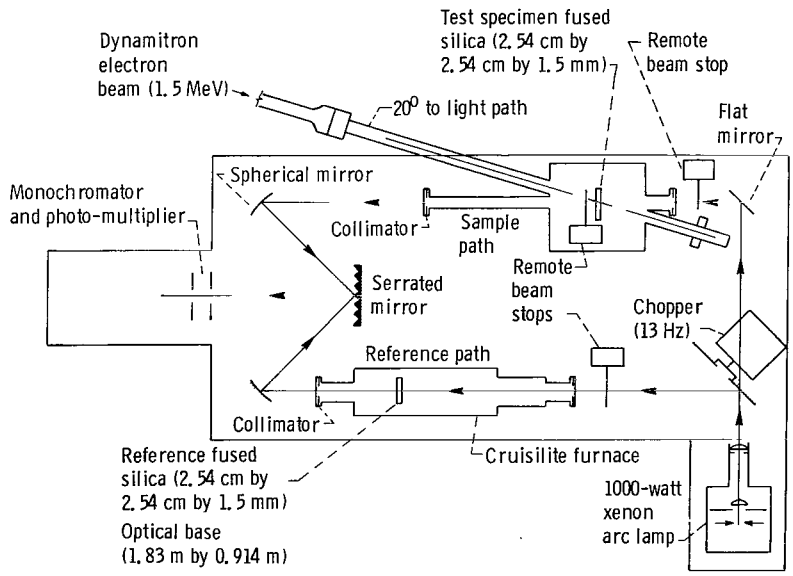

Figure 3. - Schematic diagram of reference and sample optical paths.

Before each run the electron beam alinement was checked. The procedure consisted of burning a polyvinyl chloride (PVC) plastic patch with the electron beam. One patch was attached directly to the thin aluminum window which served to separate the dynamitron beam tube and vacuum system from the sample box. Another PVC plastic patch was inserted right before the actual fused silica sample in the specimen holder. Two burns were taken, one with the sample perpendicular to the electron beam path and another at the actual test angle of 20°. In this way, the actual size and position of the electron beam was ascertained before the fused silica was tested to be certain the portion irradiated was larger than the light beam and enclosed it. Finally, a PVC plastic patch was inserted into the Faraday cup to verify that the primary electron beam impinged upon the center of the cup and not upon the secondary guard ring. After this was done, the output of the dynamitron was calibrated.

As shown in figure 3, both the test specimen of fused silica in the sample optical path and the reference specimen in the reference optical path were alined so that the respective optical beams impinged perpendicularly upon their flat parallel faces.

Lewis Dynamitron Electron Accelerator

The Lewis Research Center Dynamitron Electron Accelerator is a potential drop accelerator capable of supplying accelerating potentials between 0.3 to 3.0 MeV with voltage stability greater than 99.9 percent (ref. 1) and a beam spread of 0.1 percent. The accelerator can provide direct current, monoenergetic electrons or positive ion beams controllable from 1 microampere to 3 milliamperes. In the electron mode of operation a hot tungsten filament is used as a source of particles.

The beam transport system consists of an analyzing magnet, positioning coils, and a three element quadrupole focusing set. All power supplies for this system have sufficient stability so that the beam position changes at the output ports are less than 0.1 percent for a monoenergetic beam.

The alinement and focusing of the beam could be monitored by a beam profile monitor and also a closed circuit television system. A full-scale NLB engine operating at a radiating temperature of 8300° K is expected to give an ionizing dose rate of 5.4×10^{6} rads per second (ref. 2). This dose rate is well within the current capability of the Lewis Dynamitron Electron Accelerator.

Xenon Lamp Source and Supply

A 1000-watt xenon arc lamp was used as the primary light source. The xenon arc was maintained by a power supply which was continuously variable and was monitored to

ensure lamp performance. This power supply provided dc regulation to ±1 percent with ±10 percent change in line voltage. A fast acting control circuit compensated for changes within the lamp and produced maximum arc stability. The current ripple was 1 percent rms. A radiofrequency (rf) ignitor was used in a separate small package to allow for short rf carrying leads so it was not necessary to locate the power supply close to the lamp itself. In this way, the rf radiation that might disturb adjacent instruments was minimized. The lamp housing contained a blower for force cooling the high pressure arc lamp, allowing operation for times comparable to long NLB engine runs without any instability. The housing also contained both a spherical mirror and a ultraviolet (uv) grade fused silica condensing lens to concentrate the light beam. The spherical rear reflector imaged the arc on itself and could be adjusted while the lamp was burning. Beam light alinement could also be made while the lamp was burning. Figures 1 and 2 show the lamp source in relation to the rest of the dual beam spectrophotometer.

Dual Beam Ratio Recording Spectrophotometer

A large dual beam ratio recording spectrophotometer was designed and built to measure the transmission through the fused silica samples. This system employed two optical beams, a sample beam, and a reference beam. The two beams obtained from a single light source, are separated by using a rotating mirror beam chopper which alternately passes light to the sample mirror and to the reference path. The beams are collimated to a diameter of 0.72 centimeter which is smaller than the electron beam. The sample and the reference light beams are directed at right angles through the faces of the test and reference specimens, respectively, and are separated by approximately 45 centimeters. The two light beam paths are parallel and the geometrical path lengths from light source to the specimens are equal. They are combined by a serrated surface mirror at the entrance slit of the monochromator (see fig. 3). The rotating mirror beam chopper sequentially modulates the sample and reference beams so that locked-in signal processing techniques and phase-sensitive detection is possible. The modulating frequency is 13 hertz and the synchronizing signal obtained from the rotating mirror triggers the lock-in amplifier. Only the modulation component of the detection signal is rectified to produce a dc output from the instrument. In this way, we discriminate against the noise sources such as sample fluorescence, ambient room light, xenon lamp fluctuations, or any remaining Bremsstrahlung radiation, and are able to read an extremely weak signal superposed on this large background of noise.

The monochromator could select a particular wavelength range between 0.16 and 3.50 micrometers. Since both sample and reference beams have common detection and amplifier components and since the measurements consisted of a comparison of

sample beam intensity with reference beam intensity, inaccuracies due to amplifier gain or spectral response of the photomultiplier were reduced.

Optical Base

The xenon lamp, monochromator, mirrors and beam splitters, reference path furnace, and specimen holder box were all securely fastened to a 1-meter-wide by 2-meter-long by 3.0-centimeter-deep aluminum table with a top surface machined flat to 0.050 millimeter. Since all these parts are fixed in their relative positions, the whole base could be moved without disturbing the critical beam alinement. The complete system was then suspended from the ceiling by unistruts to completely isolate it from any vibrations caused by the vacuum pumps on the electron-beam transport system.

Electronic System

The control panel containing the phase-sensitive amplifier and the remaining electronic equipment was located in the dynamitron control room and was about 30 meters from the irradiation area. The detection system included a four-pen chart recorder which simultaneously recorded furnace temperature, specimen temperature, specimen holder temperature, and the amplified ratio between specimen and reference beams. Readout of the wavelengths and actual position of the electron beam on the specimen was accomplished by a closed circuit television camera remotely controlled from the dynamitron control console. These were monitored continuously while the test was being run. The output of the phase-sensitive amplifier was checked by viewing the signal and the rectified signal on a dual oscilloscope.

The photomultiplier tube was shielded by several lead blocks to reduce the noise generated by X-rays present during the irradiations. Low capacity signal cables were used and a line matching driver amplifier followed the preamplifier to prevent signal loss. Figure 4 shows a block diagram of the electronic setup.

This system was capable of measurement of optical transmission with an accuracy of ±1 percent. Response time was limited by the chart recorders which was approximately 1 second.

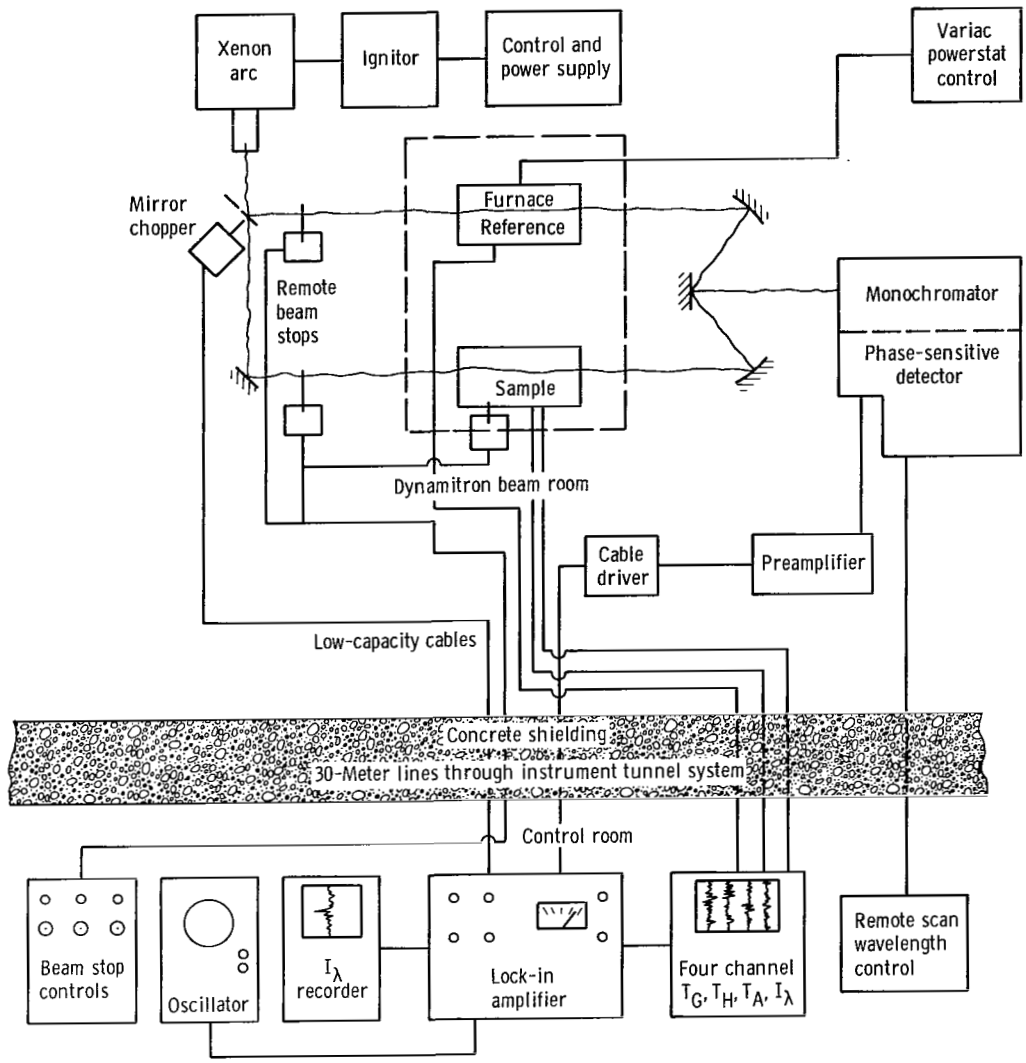

Figure 4. - Electrical and optical schematic for electron irradiation experiments.

Specimen Configuration

The specimens were wafers 2.54 centimeters square and 1.5 millimeter thick. They were polished flat to one-fourth the wavelength of sodium light and the faces were parallel to within 2 wavelengths. This shape met the various requirements of the experiment. The size of the specimens was such that the electron energy deposited gave the necessary ionizing dose rates. The specimens were thick enough to allow accurate measurements to be made of the optical transmission for absorption coefficients from 0.05 to 20 centimeters^{-1}. The specimen was alined at 20° with respect to the electron beam axis and at right angles to the optical beam axis. The optical path through it was

normal to its surface to minimize the effects of thermally induced refractive index gradients and possible temperature induced stresses which might lead to erroneous transmission determination.

Specimen Holder

The specimen is held in a metal picture-frame-type clamp. Figure 5 shows the specimen with the Chromel-Alumel thermocouple embedded in it and the thermocouple

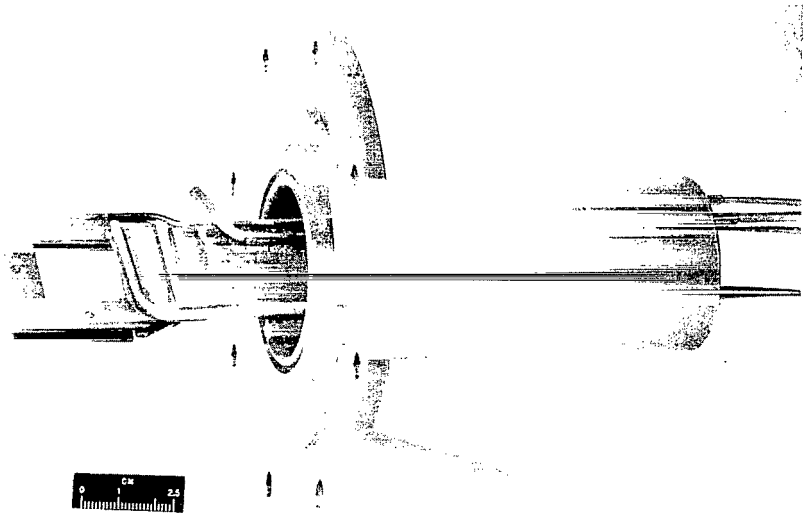

C-70-942

Figure 5. - Specimen holder.

was placed slightly above the center of the sample and wedge tightly to it by using a tapered hole through the fused silica. Spring tension of its leads and thermoexpansion of the thermocouple ball tended to secure its position throughout the test. The frame-type clamp allowed the options of hard or soft mounting of the sample. In soft mounting a ceramic gasket material was inserted between the metal holder and the fused silica for stress-free mounting. The holder had cooling slits through which a stream of helium could be blown across the faces of the specimen. At the same time cooling gas could be directed against the aluminum foil through which the electrons passed. This cooling could be omitted if desired. The foil holder was also cooled by water jackets. This double cooling could be used when very high machine currents were used. Each cooling line was valved and adjustable. The whole specimen holder assembly, which included the cooling tubes, thermocouples, and thermocouple connectors and fittings, was removable

from the sample box. It was grounded to the system to help prevent any charge buildup and repeatable positioning of the specimen was guaranteed by eight bolt holes and a centering edge. Readout of the remotely operated upstream beam stop and the thermocouples was constantly recorded during the experiment.

Sample Box

The specimen was inserted in the holder which was then bolted to the sample box. The box shown in figure 6 allowed for an air, helium, or vacuum environment for the specimen under test as required. It was connected directly to the beam transport tube but isolated from the dynamitron vacuum by a 0.05-millimeter aluminum foil. The sample box also collimated the optical light beam before and after the specimen. It could be sealed by using SiO_2 end windows. Permanent magnets were used to deflect the electron beam and to prevent the end windows from being darkened. Luminescence of the specimen during the experiment could be observed by a remote television camera through another SiO_2 port directly in line with the 20° electron beam line. By using a ZnS coating on the aluminum foil, the beam spot could also be continually monitored

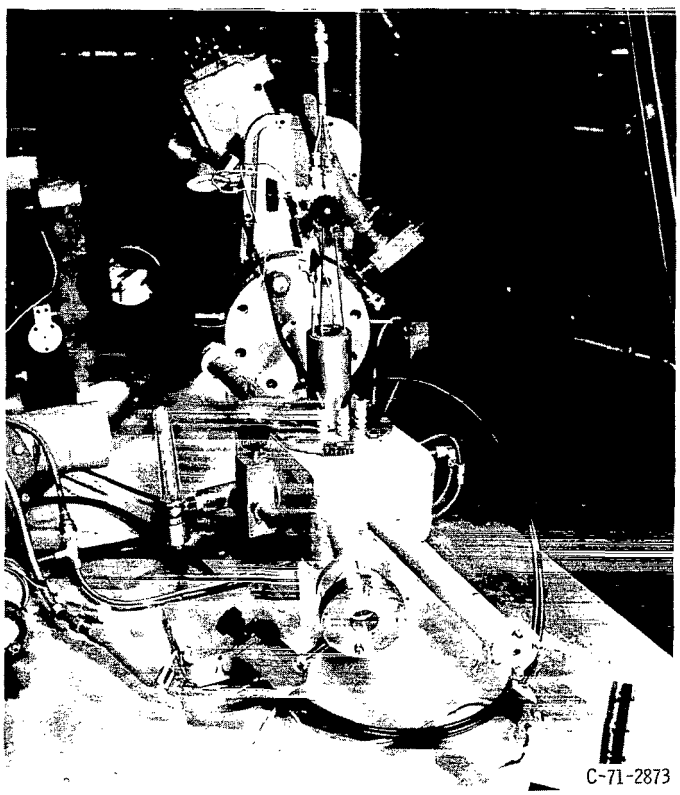

Figure 6. - Sample box.

throughout the experiment. Any beam wandering could be instantly detected. In addition the size and position of the beam spot was determined by a separate test using PVC plastic indicators at the positions of the aluminum window, sample, and the Faraday cup. This was done as a standard procedure before each test run.

Estimate of Errors

Calibration of the electron beam striking the specimen was done by removing the fused silica holder and inserting a water cooled or air cooled Faraday cup in its place. The Faraday cup was placed exactly at the same position as the specimen. The Faraday cup had a guard ring to prevent erroneous contributions from any scattered secondary electrons. This is shown in figure 7. In this way external beam current hitting the specimen was calibrated against the internal machine beam current and dial setting.

Because of the complexity of the atomic processes involved in determining the ionizing dose rate, an error of ±25 percent is estimated.

The maximum specimen temperature obtainable was governed by heating due to the electron beam, and most irradiations were done at 80- to 150-microampere-per-square-centimeter current densities. Helium cooling gas was also employed at times so that the specimen temperature was controllable downward from this maximum in the range of interest (600° to 900° C). Satisfactory temperature measurement using the Chromel-Alumel thermocouples embedded in the sample and the sample holder had an error of

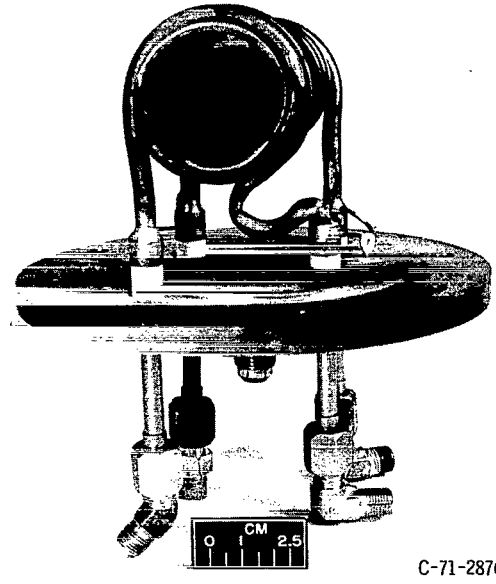

C-71-2876

Figure 7. - Faraday cup.

less than $\pm 20^{\circ}$ C based on the inherent accuracy of measuring equipment and the electron beam hitting the thermocouple. The designed spectrophotometer was capable of optical transmission measurement under laboratory conditions of ±1 percent. The overall accuracy is estimated to be of about ±16 percent at all the induced absorption coefficients of between 0.5 and 14.5 centimeters^{-1}.

ABSORPTION DATA ANALYSIS

The four-channel Bristol recorder simultaneously records specimen temperature T_S, ambient or furnace (reference specimen) temperature T_F, holder temperature T_H, and the ratio of the specimen to reference transmission signals as a function of elapsed time t. These two signals constitute the output of the phase-sensitive detector. Thus a record of transmission and temperature during the electron irradiation is accomplished. If a single test specimen was used, the light transmitted I through its flat, parallel faces is a fraction I/I_0 of the incident light I_0. The term $(1 - I/I_0)$ represents the fraction of incident light lost through absorption and reflection if interference effects are ignored.

For a specimen of thickness l and absorption coefficient α, the fraction lost through absorption is of the form $e^{-\alpha l}$. Multiple reflections in the specimen at the glass-air interface affects the total transmitted intensity. The light transmitted through the first face is $I_0 e^{-\alpha l}(1 - r)$ and $I_0 e^{-\alpha l}(1 - r)^2$ through the second face. The total transmitted intensity may be summed (refs. 3 and 4) and expressed as

$$I = I_0 e^{-\alpha l}(1 - r)^2 \left[1 - \left(e^{-\alpha l}\right)^2 r^2\right]^{-1} \tag{1}$$

where r is the reflection loss or interface reflectance, and is related to the index of refraction n by the relation

$$r = \left(\frac{n - 1}{n + 1}\right)^2$$

For fused silica in the wavelength range being considered, n does not exceed 1.6 (ref. 5); and, hence, multiple reflections can be safely ignored. So the transmission through the two interfaces of the specimen is just $(1 - r)^2$, and we may write

$$\frac{I}{I_0} = (1 - r)^2 e^{-\alpha l} \tag{2}$$

In this experiment a reference specimen was provided of the exact same composition as the test sample, in the axial cruisilite vacuum furnace of the reference optical path. This technique effectively cancels reflection losses so that equation (2) reduces to simply

$$\alpha = -\frac{1}{l}\left[\ln \frac{I(\lambda, \dot{D}, T)}{I_o(\lambda)}\right] \tag{3}$$

where $I_o(\lambda)$ is the chart recorder amplitude before the electron beam is turned on and $I(\lambda, T, \dot{D})$ is the recorder amplitude at a time t after the beam is on.

The raw data from the recorder strip chart of optical transmission, specimen temperature, and electron current density or ionizing dose rate are presented as the electron irradiation history of each specimen by converting the optical transmission to radiation induced absorption coefficient by use of equation (3) and graphing these parameters

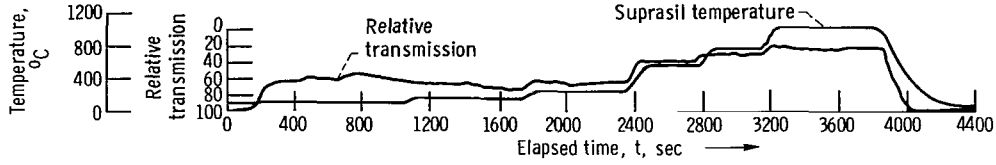

Figure 8. - Typical raw data for 1.5-millimeter Suprasil I specimen at 270.0 nanometers (2700 Å).

as a function of elapsed time. Typical raw data are shown in figure 8, in this case for a wavelength of 270.0 nanometers (2700 Å) and a Suprasil I specimen 1.5 millimeters thick.

The electron irradiation histories are shown in figures 9 to 14 for wavelengths of 215.0, 270.0, and 450.0 nanometers (2150, 2700, and 4500 Å). Data for specimens of Suprasil I and II are displayed.

CALCULATION OF ELECTRON DOSE RATES

Determining the ionizing dose rate due to the penetration of relativistic electrons into specimens which are thick compared to the range of the electron is made more complex because of the inelastic scattering and straggling of the electron energy. The electron traverses along a zigzag path due to the scattering. These two effects result in a broad distribution of electron energy loss. If the energy loss is averaged over this

broad distribution, the energy in the deposited specimen can be calculated and converted to ionizing dose rate. The useful computational scheme of Burrel, Wright, and Watts (ref. 6) which is in part based on the Monte Carlo electron transfer data of Berger (ref. 7) is used in this report and also by Palma and Gagosz (ref. 2) in their similar work on fused silica. To obtain a sufficient dose rate, it is required that the fraction of the incident electron energy deposited be as large as possible, but it is necessary to trade off this parameter with the fraction of the incident electrons actually stopping in the specimen (keeping this to a minimum so that the charge buildup in the specimen will be small). Burrel, Wright, and Watts (ref. 6) obtain expressions for the aforementioned fractions by fitting the data of Berger (ref. 8) and obtain the following semiempirical equations for normal incidence:

$$m(l, \theta) = 0.95\left[1 - \exp(-0.0653z - 2.40z^2 - 6.89z^3)\right] \tag{4}$$

$$q(l, \theta) = 0.912\left[1 - \exp(-0.0512z + 1.128z^2 - 9.38z^3)\right] \tag{5}$$

where

$m(l, \theta)$ fraction of incident electron energy deposited

$q(l, \theta)$ fraction of incident electrons absorbed in specimen

θ electron angle of incidence with specimen surface

z fraction of average path length traversed by electron in penetrating distance l

This ratio plotted against the sum of the reflection and transmission factors of Berger shows little change with variation in electron energy. The extrapolated range R(E) is approximated by

$$z = \frac{l}{(1.33 - 0.19\,E)R(E)} \tag{6}$$

where

l specimen thickness, cm

E electron kinetic energy, MeV

R(E) electron range, cm

With these considerations in mind, the specimen thickness l was chosen as 1.5 millimeters. This value permits accurate determination of the optical transmission. The range of 1.5-MeV electron in fused silica is R(E) = 4 millimeters; z is 0.36, $m(l, \theta)$ =

0.54, and $q(l, \theta) = 0.25$. Therefore, 25 percent of the penetrating electrons are absorbed giving up 54 percent of their energy in a fused silica sample 1.5 millimeters thick. The extreme complexity of the processes involved makes the relation between the ionizing dose rate $\dot{D}$ and the electron density J at a kinetic energy E of 1.5 MeV only an approximation. The relation using the technique described previously is the same one used by Palma and Gagosz (ref. 2) and is expressed as

$$\dot{D} = m(l, \theta)\left(\frac{JE}{\rho l}\right)\left[1 + \tan\beta\left(\frac{l}{\omega} + \frac{1}{3}\frac{l^2}{\omega^2}\tan\beta\right)\right]^{-1} \times 10^5 \frac{\text{rad}}{\text{sec}} \qquad (7)$$

where $m(l, \theta) = 0.54$ and the density of fused silica ρ is given as 2.2 grams per square centimeter with a specimen thickness l of 0.15 centimeter. But the actual thickness traversed by the electrons at 20° to the electron beam is 0.16 centimeter. The electron beam radius ω is 0.5 centimeter and β is the electron beam angle of divergence for fused silica of approximately 60°. With these values, equation (7) numerically reduces to $\dot{D} \cong 0.13\ J$ megarads per second as mentioned previously which was used to obtain dose rates in this report.

EXPERIMENTAL RESULTS

The results of a run in which the optical transmission of a 3.00-millimeter Suprasil II specimen was measured during the irradiation at a wavelength of 215.0 nanometers (2150 Å) is presented in figure 9. At the dose rate of about 10 megarads per second there was evidently a loss in transmission, and the induced absorption coefficient α was almost 8 centimeters^{-1}. This was seen even though the temperature reached the high value of 1000° C. Similar tests were run at wavelengths of 270.0 and 450.0 nanometers (2700 and 4500 Å) using 3.00-millimeter-thick Suprasil II samples. The electron irradiation history of these samples is shown in figures 10 and 11.

Generally, as the dose rate increased, both the temperature and the induced absorption coefficient increased. The temperature followed the dose rate as expected, and the equilibrium value for the induced absorption coefficient was about 5 centimeter^{-1} for the specimen at 270.0 nanometers (2700 Å). At 4500 Å this trend was also obvious, but it should be noted that the induced absorption coefficient did decrease with rising temperature more than at 215.0 or 270.0 nanometers (2150 or 2700 Å). At these two wavelengths the prolonged high temperature actually warped the specimens and no return to a low absorption coefficient was seen when the electron beam was shut off. This was guarded against in the 450.0 nanometers (4500 Å) run and did not occur. The thickness of these specimens was greater than that which was necessary to ensure the deposit of a large

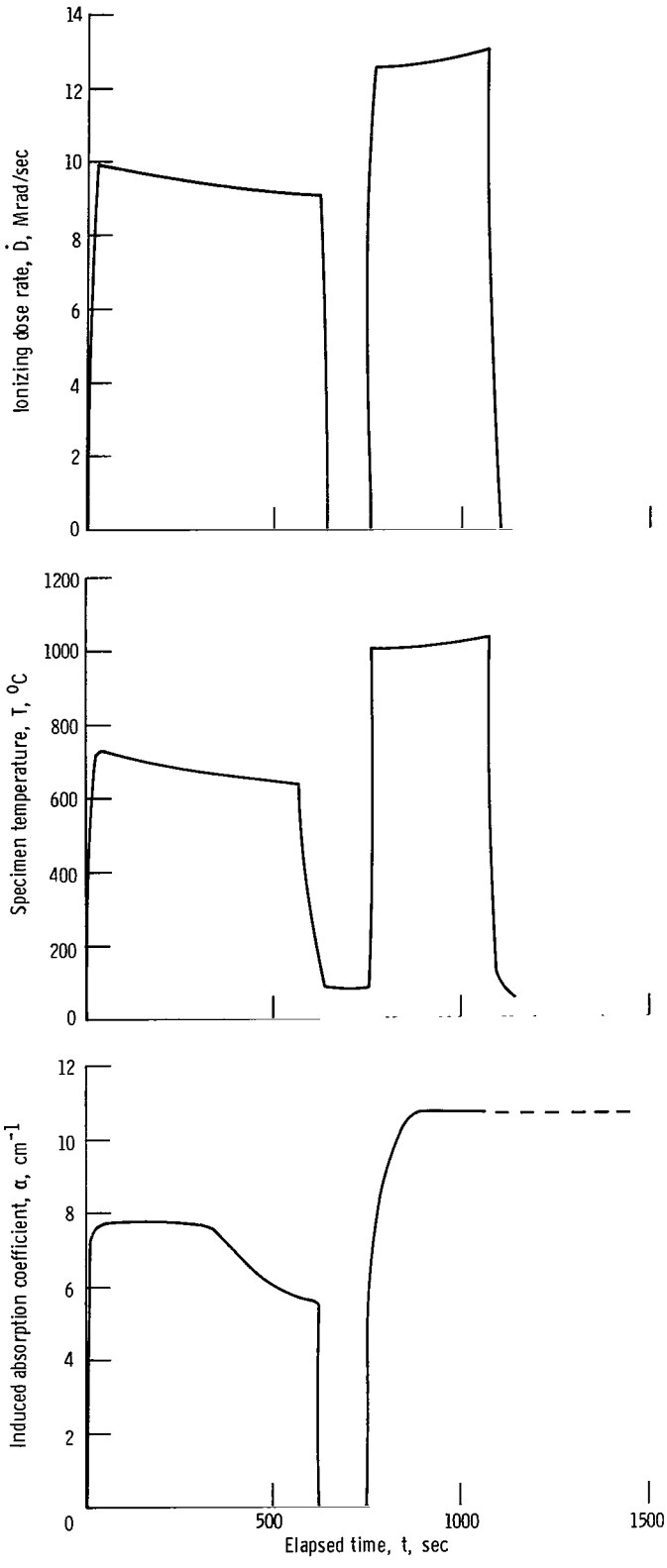

Figure 9. - Electron irradiation history of 3.00-millimeter Suprasil II specimen at 215.0 nanometers (2150 Å).

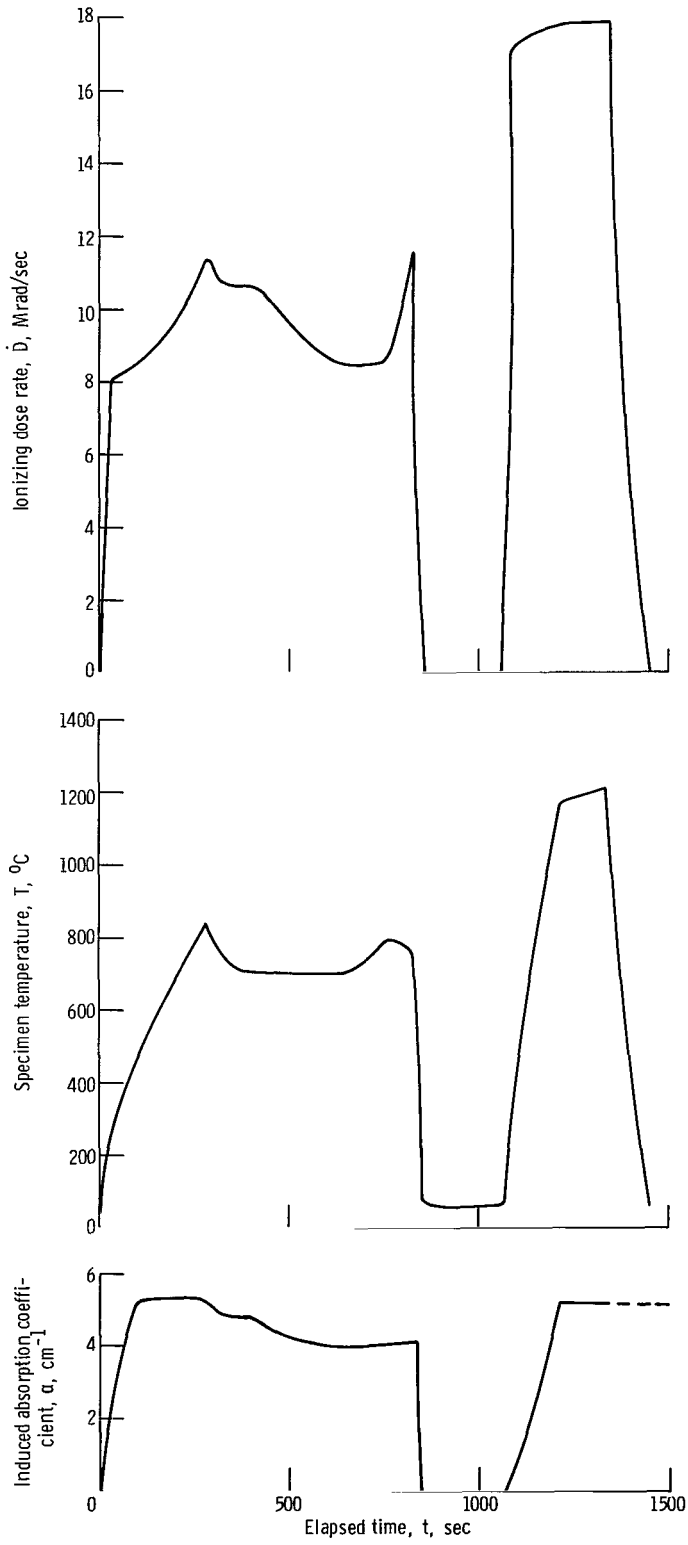

Figure 10. - Electron irradiation history of 3.00-millimeter Suprasil II specimen at 270.0 nanometers (2700 A).

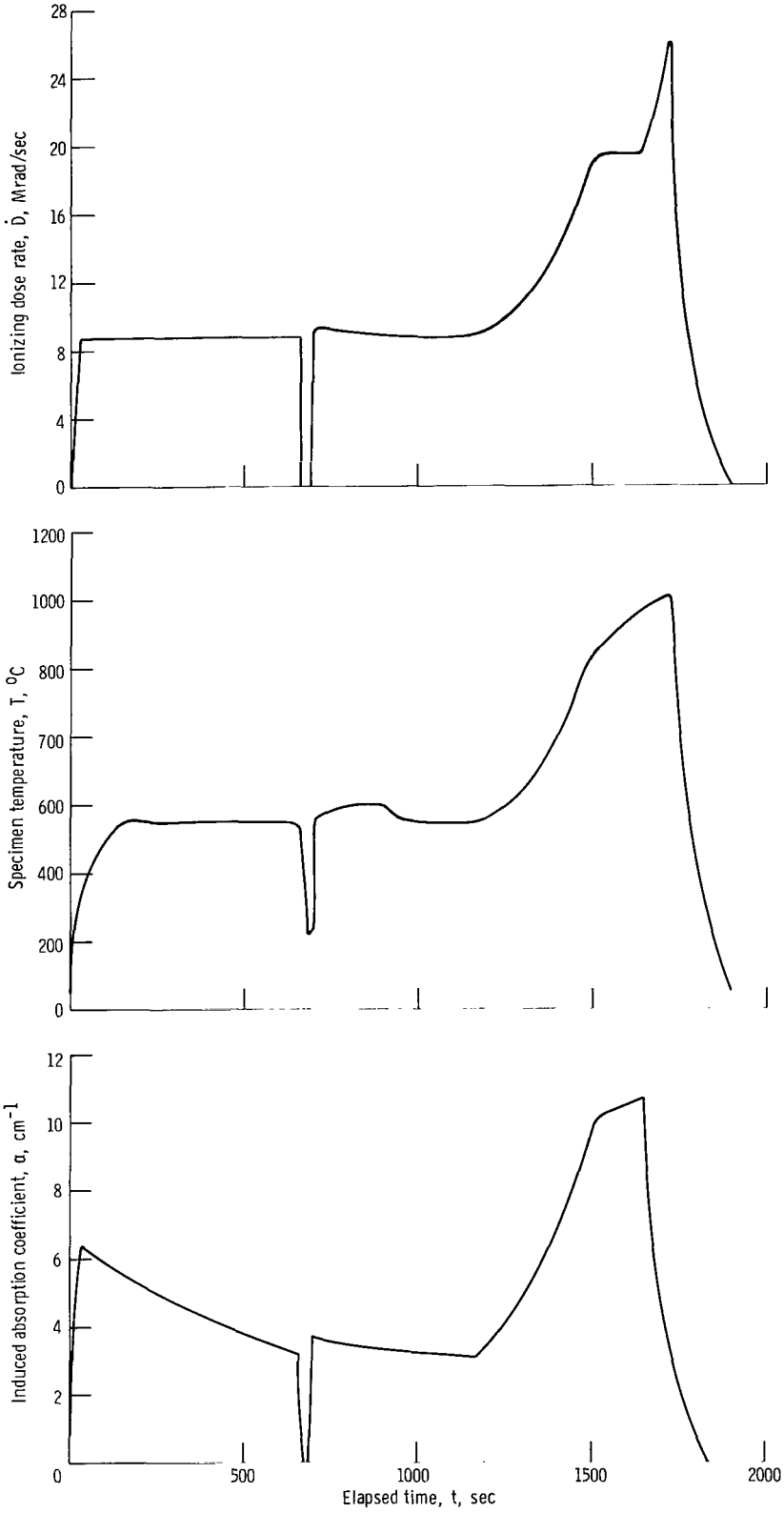

Figure 11. - Electron irradiation history of 3.00-millimeter Suprasil II specimen at 450.0 nanometers (4500 Å).

fraction of incident electron energy. Since the fraction of the incident electrons actually stopping in the specimen was also large, there could be a large charge buildup which could cause dielectric breakdown. A better compromise between these contradictory requirements was met by reducing the specimen thickness to 1.5 millimeters as explained under specimen configuration. Subsequent test runs were made with these 1.5-millimeter samples.

Figure 12 presents the electron irradiation history of a 1.5-millimeter Suprasil I specimen at 215.0 nanometers (2150 Å). Here the ionizing dose rate is raised in step intervals. It can be seen that both the temperature and the absorption coefficient is increased correspondingly and that the temperature does lie in the range of interest. For very high dose rates and temperature the absorption coefficient fails to show this high peak, and α has attained about half the maximum value under the lowest dose rate used.

There is an almost indiscernible decrease in this absorption coefficient in time at this temperature. Generally, the induced absorption coefficient is decreased very slight-

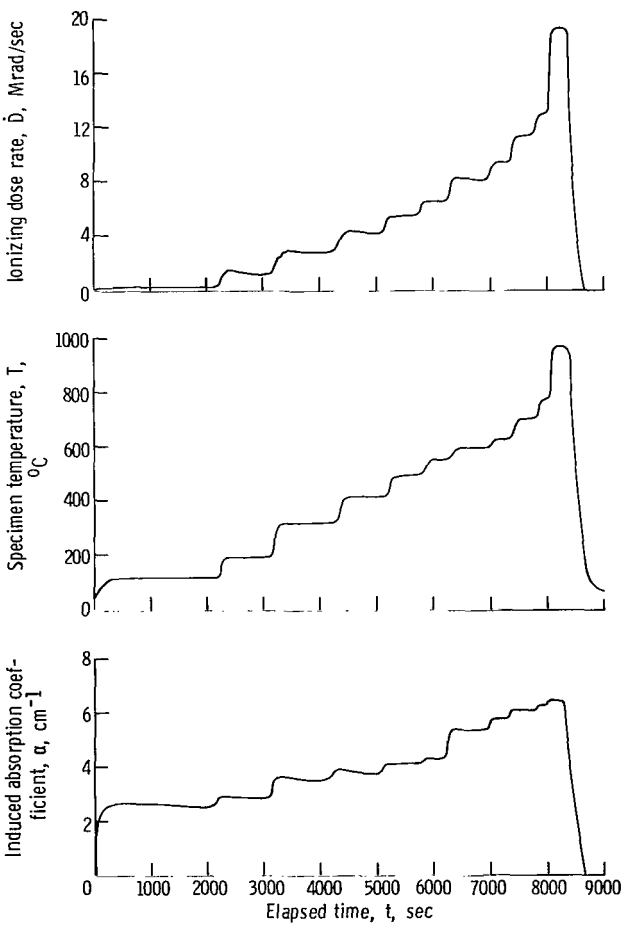

Figure 12. - Electron irradiation history of 1.5-millimeter Suprasil I specimen at 215.0 nanometers (2150 Å).

ly from its initial value at the outset of the irradiation but does not go to very low values until the bombardment is stopped. A corresponding decrease is noted in the ionizing dose rate.

Although 215.0 nanometers (2150 Å) is the wavelength of primary interest, the temporal behavior at 270.0 and 450.0 nanometers (2700 and 4500 Å) was also investigated. The results at 270.0 nanometers (2700 Å) are shown in figure 13. The curves of the ionizing dose rate, temperature, and induced absorption coefficient of the Suprasil I specimen are very similar to those exhibited by the Corning 7940 UV specimens, so the results for the latter are not shown. Plateaus of these parameters except as shown in figure 13 at approximately 1000 seconds seem to follow the level of the dose rate employed with no real decay of the absorption coefficient as the temperature is increased by increased irradiation dose. This decided decrease in the induced absorption coefficient at about 1000 to 2000 seconds shown in figure 13 is probably due to the thermal annealing rate which is larger than the coloration rate at this small ionizing dose rate.

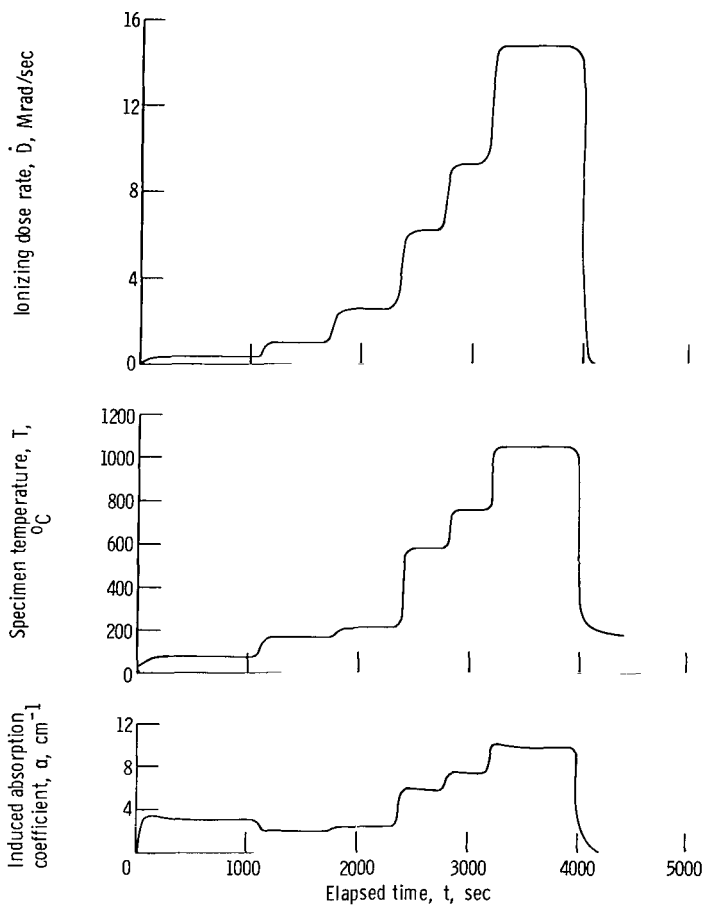

Figure 13. - Electron irradiation history of 1.5-millimeter Suprasil I specimen at 270.0 nanometers (2700 Å).

The results of the optical transmission of a Suprasil I specimen during irradiation at wavelengths of 450.0 nanometers (4500 Å) are presented in figure 14. It is expected that this curve would be different from those at the previous wavelengths since neither Corning 7940 UV nor Suprasil I fused silica has any strong irradiation-induced absorption bands at the 450.0 nanometers (4500 Å) wavelength. Even without a strong absorption band at this wavelength, at the offset of this test run (0 to 50 sec) the specimen sustained enough damage to display a large transmission loss at the starting dose rate. But, as soon as the temperature reached a point high enough so that the thermal annealing rate became dominated, the curve rapidly turned down. Accordingly, it is no surprise to see, at a steady-state dose rate with a steady temperature of 400^{o}C maintained, that the induced absorption coefficient shows a sharp rise and then decays rapidly to a steady lower value until the beam is shut off. The curious bump in the induced absorption curve at the end of the run is due to a sudden burst of electrons from the dynamitron during a spark out. The subsidiary peak seen at the wavelength of 270.0 nanometers (2700 Å) displayed the same general behavior for Suprasil I and Corning 7940 UV specimens as shown at the wavelength of 215.0 nanometers (2150 Å).

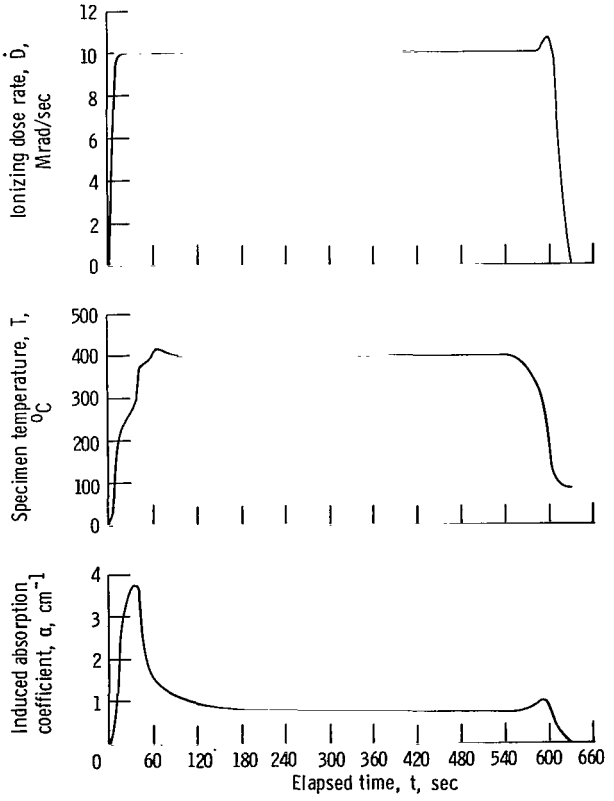

Figure 14. - Electron irradiation history of 1.5-millimeter Susprasil I specimen at 450.0 nanometers (4500 Å).

Table I summarizes the representative data of the equilibrium values of the irradiation-induced absorption coefficient at the wavelengths of 215.0, 270.0, and 450.0 nanometers (2150, 2700, and 4500 Å). Both 3.0- and 1.5-millimeter-thick specimens are tabulated along with the ionizing dose rate, specimen temperature due to electron beam heating, and the fused silica type.

TABLE I. - SUMMARY OF EQUILIBRIUM VALUES AT 215.0, 270.0, AND 450.0 NM

Specimen	Specimen type	Wavelength, nm	Specimen thickness, mm	Temperature, ^{o}C	Dose rate, Mrad/sec	Induced absorption coefficient, cm^{-1}
1	Suprasil I	215.0	1.50	110 to 970	0.2 to 19.0	3 to 6.5
2	Corning 7940 UV	↓	↓	950	18.0	5 to 1.2
3	Corning 7940 UV			345	5.5	3.5
4	Corning 7940 UV			500 to 580	11.0	6 to 4.0
5	Corning 7940 UV (soft mount)			250 to 1050	2.6 to 24.0	2.2 to 14.3
6	Suprasil I	270.0		80 to 1000	0.2 to 14.7	3 to 9.7
7	Corning 7940 UV	270.0		200	4.0	3.3
8	Corning 7940 UV	270.0		550 to 430	8.3 to 5.5	7 to 5.0
9	Suprasil I	450.0		400	10.0	3.7 to 0.8
10	Corning 7940 UV	450.0	↓	600 to 1000	14.7 to 11.7	1.5 to 0.5
11	Suprasil II	215.0	3.00	700	9.0 to 10.0	8 to 10.5
12	Suprasil II	215.0		1000	12.5 to 13.0	10.7
13	Suprasil II	270.0		1200	18.0	5.2
14	Suprasil II	270.0		700	8.0 to 11.5	4 to 5.0
15	Suprasil II	450.0		550	8.8	6.3 to 3.2
16	Suprasil II	450.0	↓	1000	8.8 to 24.0	10.7

BACKGROUND OF IRRADIATION-INDUCED OPTICAL ABSORPTION IN FUSED SILICA

Extensive investigation of the effects of radiation on fused silica have been made, and it was found that fused silica is colored both by ionization radiation and by high energy particles capable of displacing lattice atoms. Although there has been much effort spent in the area of optical absorption, the former lack of appreciation of the role of chemical impurities and the absence of a good theoretical model for a defect in a solid where the binding is partially covalent and partially ionic have slowed progress. The experimental work in this report has been done using very high quality fused silica. Commercial grades of fused silica when exposed to neutrons and other ionizing radiation exhibit a large number of optical absorption bands in both the visible and ultraviolet wavelengths. Most of these absorptions seem to be due to impurities. In this work, Suprasil I and II and Corning 7940 UV fused silica are used. Corning 7940 UV is essen-

tially free of most impurities but has a controlled water content of approximately 0.1 percent and an appreciable amount of OH radicals. Studies of the optical absorption by many investigators of neutron-irradiated fused silica have uncovered bands at 550.0 nanometers (2.26 eV), 300.0 nanometers (4.15 eV), and 215.0 nanometers (5.8 eV) (ref. 9). In the nomenclature of Mitchell and Paige (ref. 10), these are the A-, B-, and C-bands, respectively. Also noted is a weak band at 260.0 nanometers (4.8 eV) which has been called the B_2-band. The availability of the ultrahigh purity fused silica used in this experiment gives considerable help to studies of defect-associated optical bands. This fused silica exhibits a single irradiation-induced absorption band which is centered at 215.0 nanometers (2150 Å) and subsidiary peaks at 270.0 and 450.0 nanometers (2700 and 4500 Å). It appears to be the most resistant to coloration by electron bombardment (ref. 10).

The intrinsic absorption edge or E-band (refs. 10 and 11) at approximately 165.0 nanometers (1650 Å), where fused silica becomes essentially opaque, was not investigated here, but it may have been produced, and if so, could have considerable influence on the feasibility or practicality of the NLB concept. The slower growth of the absorption band at 215.0 nanometers (2150 Å) in Corning 7940 UV may be due to the quenching mechanism by the water content. The details of this quenching mechanism is not known, but the generation of the irradiation-induced absorption band at 215.0 nanometers (C-band) in fused silica is described by Mitchell and Paige (ref. 10) as an electron trapped in an oxygen vacancy, and the 165.0 nanometers (E-band), by a hole trapped at an interstitial oxygen ion. This two step process requires the presence of a particular defect in the structure of the glass which can be generated in several ways. The fact that no substitutional impurity is involved reduces the defect possibilities and simplifies this study. The generation of this positively charged $(SiO)^+$ ion or defect could result from an incident neutron removing an oxygen ion from the SiO_2 molecule. The displaced oxygen ion, separated by many atomic distances from the positively charged $(SiO)^+$ ion, creates a vacancy interstitial pair. A cascade process can occur since a large amount of kinetic energy could be given to the oxygen ion, thereby producing many additional defects.

Another model of the C-band has been suggested. Nelson and Crawford (ref. 12) suggest that a center may arise from a partial valence bond localized either on a silicon or an oxygen atom. This model is based on the rupture of Si-O bonds with the formation of free radicals as a principal product. The removal of an electron from a strained Si-O bond makes it possible for the atoms to settle in new equilibrium positions which stabilize the center. We see that the Mitchell and Paige model requires that an oxygen ion be displaced from its lattice site, whereas the Nelson and Crawford model does not.

Ionizing radiation such as electrons or gamma rays can also generate these defects by breaking the silicon-oxygen bond in the SiO_2 molecule. A negatively charged O^- ion displaced only slightly from the positive $(SiO)^+$ ion is the result. Work by Compton and

Arnold using high energy electrons (ref. 13) on Corning 7940 UV and Corning 7943 UV show that defects which give rise to the C-band (215.0 nm) are generated by an ionization process. Corning 7940 UV contains an appreciable amount of OH^- whereas Corning 7943 UV is virtually free of OH^- ions. They conclude that the defect formation occurs by ionization processes in the water-free fused silica (Corning 7943 UV) but that the presence of water not only induces an additional absorption band 257.0 nanometers (2750 Å), but affects the damage mechanism, and the situation is less understood in Corning 7940 UV material. Although the role of the water impurity is not understood, no evidence that direct displacements are required to generate the C-band, even in this material, was found. Obviously the nature of the material is of great importance, in measuring absorption bands. Unfortunately at the beginning of this experiment we were unaware of these differences.

In studies (ref. 13) of highly ordered crystalline quartz the 215.0-nanometer (2150 Å) band is found only after irradiations where there has been sufficient disruption of the crystalline structure to generate appreciable numbers of stable broken valence bonds. In fused silica a significant concentration of defects may be present due to the intrinsic disorder in the glass structure, but only a small number of electrons are free to be trapped at these defects. But, the electron beam or other ionizing radiation creates a large number of free electrons that are available to be trapped at the positively charged defects. This result is believed to be responsible for the irradiation-induced absorption band in fused silica centered at 215.0 nanometers (2150 Å). This complex is referred to as a color center, which is in the ultraviolet wavelength. Thus, ionization can create defect centers without actually displacing atoms. It is felt that a realistic model of radiation produced defects in quartz and fused silica must await a careful study of the vacuum ultraviolet region, and in addition to optical absorption measurements corollary studies, such as paramagnetic resonance and magnetic suspectibility on various forms of silica are vital to the correct interpretation of color centers in the silica system.

DEFECT REMOVAL

Thermal Annealing

Decoloration of radiation damage fused silica occurs at various temperatures. The color centers for the absorption band at 215.0 nanometers (2150 Å) are stable at ambient temperatures. It appears that several processes may be effective in annihilating these color centers. Some studies have shown that decoloration due to heating cover two ranges of behavior. Trapped electrons in the centers are liberated by nearby thermal vibrations and thermal bleaching results, wherein partial removal of the color center is

accomplished but the trapping centers are not destroyed. Mitchell and Paige (ref. 10) found that this process called thermal bleaching occurs below 500° C. The second range, above 500° C, results in complete annihilation of the color center trap and a recombination of the $(SiO)^+$ ion with an O^- ion can occur. This process is called thermal annealing, and is apparently complete at 950° C. The defect-annealing process at higher temperatures is complex and a broad spread of activation is indicated. It has been found on annealing Corning fused silica specimens previously exposed to fast neutrons that the C-band normally decreases but the E-band is not seriously affected. The atmosphere surrounding the specimen during the high temperature annealing or impurities may also influence the annealing. Some studies show that thermal annealing can cause different absorption bands to be bleached at different rates and can increase some bands at the expense of others. As noted by Ditchburn et al. (ref. 8), in some fused quartz certain absorption bands appear if the sample is heat treated prior to irradiation that are not seen if there is no heat treatment. This has been observed by van Wieringen and Kats (ref. 9) and others. Obviously, there is great complexity present when there is both disordering due to radiation and thermal annealing of these disordered products simultaneously as in the present experiment. The possible formulation of different annealing processes in several stages implies competing processes in the irradiated specimens, and it may be expected that the results will depend on the conditions and annealing treatments.

Optical Bleaching

Optical bleaching of coloration in fused silica, where light is absorbed by the color center which can result in the liberation of a trapped electron, also occurs. Optical bleaching is a function of both spectral distribution and intensity of the bleaching light. Fused silica which has been γ-irradiated is difficult to bleach optically and only after prolonged exposures to ultraviolet have reductions by a factor of three or four been noted by Levy and Varley (ref. 14). The temperature at which optical bleaching is performed is important with efficiency very reduced at low temperatures. They combined optical and thermal bleaching at 250° C and showed that the combination is highly efficient in removing coloration in fused silica. They found that the C-band was very resistant to optical bleaching after neutron exposure. The explanation of this thermal assistance to optical bleaching may be that there is thermal destruction of the defect or that thermal vibrations help excited electrons escape to the conduction band. No clarification of this is attempted in this experimental work as optical bleaching was not studied at this time.

Radiation Bleaching

The complex nature of defect structures in fused silica has been shown by the numerous optical absorption bands developed by γ, X-ray, neutron and high energy electron irradiation. Mitchell and Paige (ref. 10) and Levy and Varley (ref. 14) mention that continuous radiation by pile neutrons can bleach the A- and B-bands in some samples of fused quartz. At the same time there is an apparent shift in the C-band maximum towards higher energies.

This is attributed to vacancies caused by atomic displacements combining with electron traps to produce new centers, which are assumed to give an absorption in another band. It is to be noted that this work was done on "Vitreosil" a fused quartz with sodium borate impurities in the glass (ref. 10). Mitchell and Paige noted that any radiation bleaching in quartz must be by neutrons and suggested that it might be caused by a transmutation of aluminum by thermal neutrons or the displacement of aluminum or some neighboring atoms. Experiment did bear this out, however, and they concluded that the ratio of absorbing centers to concentrations of defects for a given type of radiation depends on the relative occupancy of the other trapping centers, and might provide a basis for a mechanims of radiation bleaching.

In our experiment which used high energy electrons instead of neutrons on high purity fused silica, there was absolutely no evidence of radiation annealing. Since we believe that ionization effects, rather than displacement effects, are responsible for the color in our fused silica, we were not surprised at the absence of any enhancing of the annealing process by any phenomenon such as radiation annealing. Certainly this effect would have been evident under the conditions of high temperature and large dose rates used in our tests.

DISCUSSION

This experimental study attempted to determine the level of the irradiation-induced absorption expected in the transparent wall of the nuclear light bulb (NLB) engine when the wall is kept at elevated temperatures. The data pertaining to the optical transmission of Corning 7940 UV and Suprasil I and II fused silica established the behavior of the induced absorption coefficient as follows:

In irradiations conducted at 215.0 nanometers (2150 Å), the wavelength of primary interest, the irradiation-induced absorption coefficient reached a steady-state value once the specimen temperature had stabilized.

Raising the electron current density or ionizing dose rate caused the induced absorption coefficient to increase to a higher steady-state value despite the fact that (for constant cooling) the temperature was raised concurrently with the dose rate.

Increasing the temperature of the specimen while maintaining the same ionizing dose rate resulted in a lower value for the irradiation-induced absorption coefficient to a lower steady-state value.

The irradiation-induced absorption coefficient decreased rapidly after the electron beam was turned off. The small hump appearing in some of the curves is caused by the response of the recorder.

The trends shown by the 3.0-millimeter specimens were similar to the 1.5-millimeter specimens except the thicker specimens tended to reach the high temperatures quicker than the thinner specimens with less beam impinging upon them. Accordingly, they probably experienced more thermal stress. This investigation showed that Corning 7940 UV and Suprasil I at the wavelengths of 215.0, 270.0, and 450.0 nanometers (2150, 2700, and 4500 Å) are approximately the same. No significant differences attributable to temperature effects was noticeable between these two materials.

Values ranging from 14.5 to 2.2 centimeter^{-1} were recorded for the irradiation-induced absorption coefficient at the wavelength of 215.0 nanometers (2150 Å) depending upon the test conditions.

At the wavelength of 270.0 nanometers (2700 Å) both types of specimens exhibited essentially the same behavior as stated above at 215.0 nanometers (2150 Å). The induced absorption coefficient varied between 3 to 9.7 centimeters^{-1} depending on the test conditions. Similar trends were seen for the 3.00- and 1.5-millimeter thick samples.

The response at the 450.0-nanometer (4500 Å) wavelength displayed less transmission loss than at the wavelengths of 270.0 or 215.0 nanometers (2700 or 2150 Å) as expected. In addition the induced absorption coefficient rose to a maximum value and then decayed rapidly to a lower steady-state value. This transient change in transmission was expected since this fused silica used does not exhibit any strong absorption bands at 450.0 nanometers (4500 Å) and any damage sustained by the fused silica would be quickly annealed.

There was some question as to whether heating the specimen by the electron beam could produce an apparent loss of optical transmission by stresses in the specimen which thereby displace the optical beam off the monochromator slit. In order to test this possibility of a thermal effect erroneously giving a loss in optical transmission, tests were run at 300.0 nanometers (3000 Å), a wavelength at which the induced absorption was negligible. Three runs were made using 1.5-millimeter samples of Corning 7940 UV fused silica. One test was performed in open air, one with the sample box evacuated, and one with helium. The results shown in figure 15, clearly show there was no anomaly due to specimen temperatures even though very high temperatures were reached by the test sample.

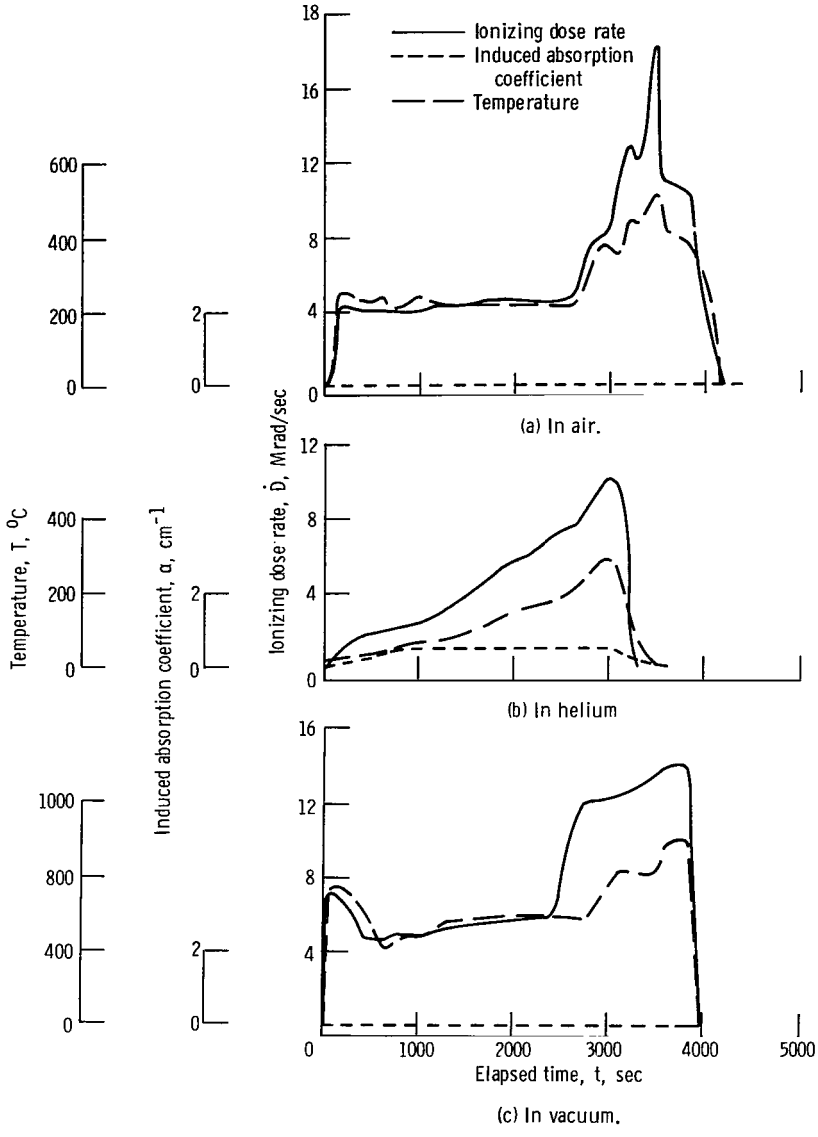

Figure 15. - High temperature tests for absorption anomaly of 1.50-millimeter Corning 7940 UV specimen at 300.0 nanometers (3000 Å).

Note that there is some absorption seen in the helium environment. This is caused by the helium gas flow which kept the specimen temperature down and forced a steady-state condition between thermal annealing and radiation induced coloration which produced the small transmission loss.

A Corning 7940 UV specimen was soft mounted using a special ceramic material in order to remove any doubt that thermal strains imposed by the sample holder might give erroneous results. The wavelength of the test is 215.0 nanometers (2150 Å), and no significant difference in the results are evident using this ceramic soft mounting material. All parameter trends are repeated and verified and are displayed in figure 16.

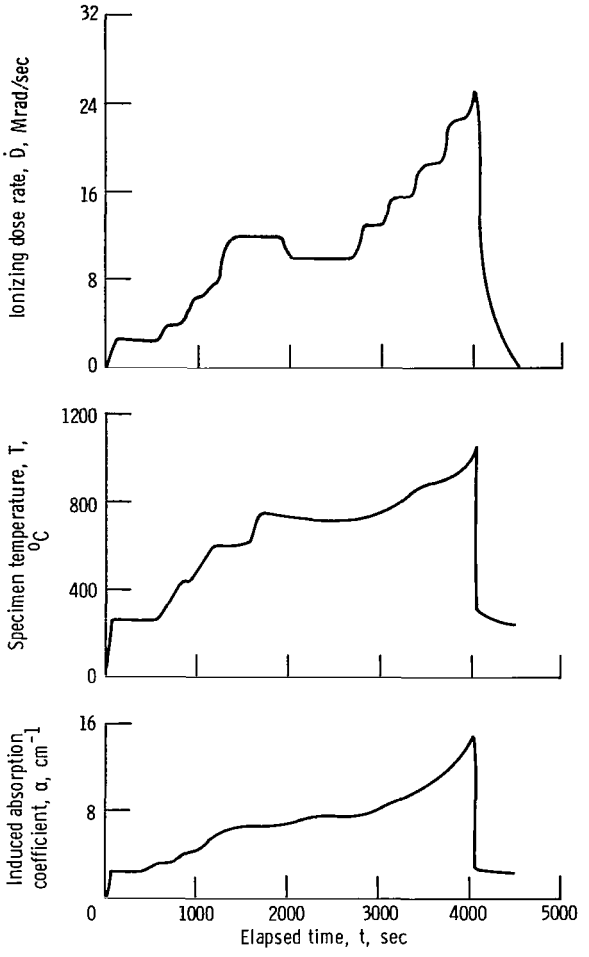

Figure 16. - Electron irradiation history of 1.5-millimeter Corning 7940 specimen at 215.0 nanometers (2150 Å). (Soft mounted and air environment.)

The steady-state irradiation-induced absorption coefficient at 215.0 nanometers (2150 Å) over temperatures ranging from 100^{o} to 1000^{o} C are plotted against the ionizing dose rate in figure 17. Data from our investigation are shown together with the data from a similar experiment conducted by Palma and Gagosz in reference 15. It is apparent that there is evidence of disagreement in these two experiments. The claim of Palma and Gagosz that the induced absorption coefficient at a given temperature first rises with increasing dose rate, reaches a maximum value, and then begins to decrease with increasing dose rate is not verified by this experimental work. Although this work has been done with specimens of the same size, composition, and configuration, the results, as presented by this graph, differ markedly. A thorough examination of their apparatus has failed to reveal to us the cause of this discrepancy.

There were several differences between our experimental arrangement and the ex-

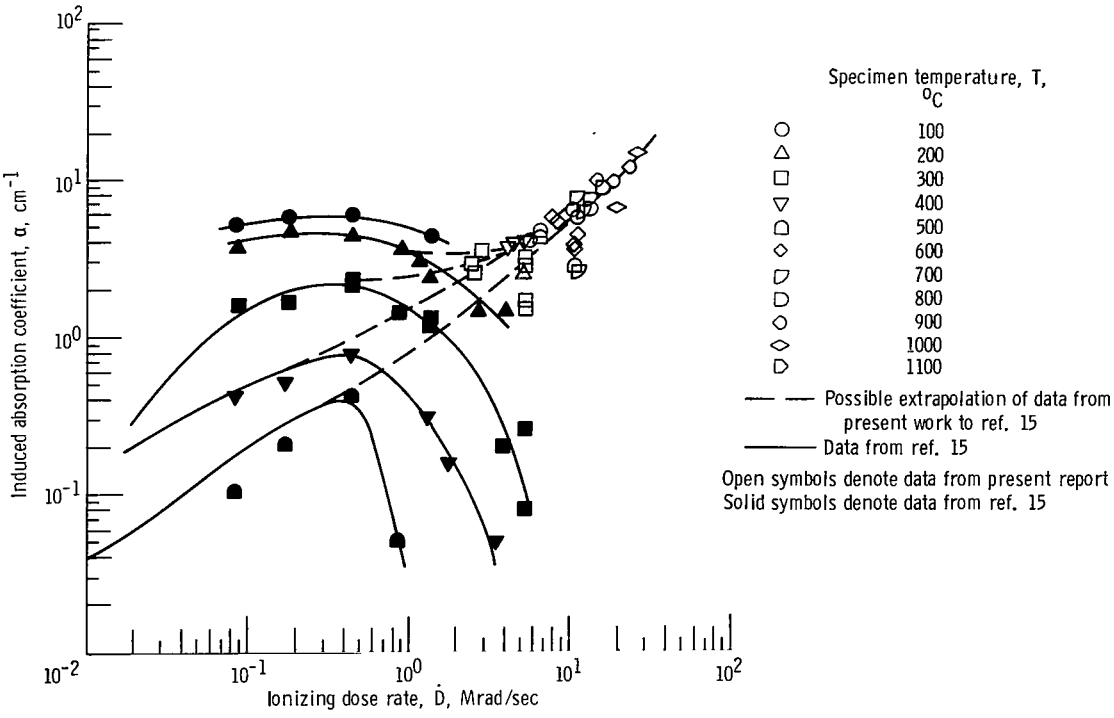

Figure 17. - Steady-state induced absorption coefficient at 215.0 nanometers (2150 Å).

perimental setup of Palma and Gagosz (ref. 15). They were able to obtain data at a fixed temperature and various doses, as well as at fixed doses and various temperatures by using an auxiliary furnace in their test section. This permitted them to get data at a higher temperature and lower dose rate. Although our experiment did permit a decrease in temperature (by cooling) at a given dose for low doses, we could not increase the temperature above that due to heating by the electron beam. This restricted the direct comparison between our results and the results of Palma and Gagosz to a narrow range of temperature and dose rate.

The dashed curves connecting the two different sets of data show one attempt at bridging these differences. It represents an extension from their data at the lower dose rate to ours at a higher dose rate and shows how the curves would appear if the induced absorption coefficient would not decrease due to radiation annealing. We did not investigate the intrinsic absorption edge or E-band (refs. 10 and 11) at approximately 165.0 nanometers (1650 Å), where fused silica becomes essentially opaque. Nonetheless, it may have been produced, and if it was, it could have a great effect on the feasibility of the NLB concept.

CONCLUSION

The primary objective of this investigation was the measurement of the level of irradiation-induced optical absorption and the resulting heat deposition in the wall material separating the fuel and the propellant of the nuclear light bulb (NLB) engine.

The Lewis Research Center dynamitron provided the equivalent ionizing radiation and high temperatures that the transparent gas divider of the NLB would experience. Radiation times were sufficient so that equilibrium between radiation induced coloration and high temperature annealing was reached.

The most likely candidates for this wall material was fused silica and samples of Corning 7940 UV and Suprasil I and II were tested. The electron beam heated the fused silica to temperatures ranging from 150° to 1000° C. A special dual-beam spectrophotometer constructed to make these equilibrium transmission determination's measured the optical absorption at the wavelength of 215.0 nanometer (2150 Å) which is the center of the irradiation induced absorption band in fused silica, and at the additional wavelengths of 270.0 and 450.0 nanometers (2700 and 4500 Å).

The experimental results indicate the behavior of the induced absorption coefficient as follows:

1. At 215.0 nanometers (2150 Å) the irradiation-induced absorption coefficient reached a steady-state value after temperature stabilization of the specimen.

2. Despite the fact the temperature was raised with increase in dose rate or the electron current density, the induced absorption coefficient increased to a higher steady-state value.

3. If the ionizing dose rate was kept constant and the specimen temperature was increased, a lower steady-state value for the irradiation-induced absorption coefficient resulted.

4. There was rapid decrease of the irradiation-induced absorption coefficient after the electron beam was turned off.

5. Equilibrium values of the induced-absorption coefficient at 215.0 nanometers (2150 Å) range from 14.5 to 2.2 centimeters^{-1}, at 270.0 nanometers (2700 Å) the values were 9.7 to 3.0 centimeters^{-1} and at 450.0 nanometers (4500 Å) this range was 3.7 to 0.5 centimeters^{-1}. No significant difference was noted between Suprasil I and II and Corning 7940 UV. Similar results were shown for specimens of 1.5- and 3.0-millimeter thickness. No anomaly due to specimen stress at these elevated temperatures was indicated whether the specimens were soft mounted using a ceramic gasket or firmly mounted.

This particular investigation does not give a complete answer as to the practical realization of the NLB propulsion scheme. An extension of this study to include the effects of optical bleaching, absorption in the vacuum ultraviolet wavelength region of

165.0 nanometers (1650 Å), wavelength scans over the range of 200.0 to 300.0 nanometers (2000 to 3000 Å), additional test for any anomaly due to high temperature, and the temporal behavior and measurements of the irradiation-induced optical absorption of other promising transparent wall materials such as aluminum oxide, beryllium oxide, and titanium oxide should be performed. Since the objective of the present investigation was to measure under simulated reactor environment, at the wavelengths of interest, the optical transmission of fused silica, it is desirable to simulate the actual test conditions as accurately as possible. Therefore, it would be advantageous to extend this work also by utilizing the high energy proton beam soon to be available from the modified Lewis Research Center cyclotron. This accelerator will provide protons in the energy range of 10 to 55 MeV and running times which will produce the equivalent ionizing radiation and temperatures of a full-scale operating NLB engine and particularly simulate neutron damage in the specimen. Although there are still areas, as shown previously, needing attention in this work, the results of the present investigation indicates significant optical absorption at the wavelengths of interest. This conclusion implies that the feasibility of this concept insofar as it depends upon fused silica transparency under these conditions is open to question.

Lewis Research Center,
National Aeronautics and Space Administration,
Cleveland, Ohio, April 11, 1972,
112-02.

APPENDIX - SYMBOLS

$\dot{D}$	ionizing dose rate, Mrad/sec
E	electron kinetic energy, MeV
I	transmitted light intensity, W/cm^2
I_o	incident light intensity, W/cm^2
I/I_o	fraction of incident light
D_λ	chart recorder amplitude prior to irradiation
$I(\lambda, T, \dot{D})$	chart recorder amplitude during electron irradiation at time t
J	electron current density, $\mu A/cm^2$
ℓ	optical path length through specimen or specimen thickness, cm
n	index of refraction
$m(\ell, \theta)$	fraction of incident electron energy deposited
$q(\ell, \theta)$	fraction of incident electrons absorbed
R(E)	electron range, cm
r	reflection loss or interface reflectance
T	specimen temperature, ^oC
T_A	ambient temperature, ^oC
T_F	furnace temperature, ^oC
T_G	temperature of fused silica, ^oC
T_H	fused silica holder temperature, ^oC
T_S	fused silica specimen temperature, ^oC
z	ratio between specimen thickness and average path length
α	irradiation-induced absorption coefficient, cm^{-1}
β	electron beam angle of divergence, deg
θ	electron angle of incidence with specimen surface, deg
λ	optical wavelength, Å
ρ	density of fused silica, g/cm^3
ω	electron beam radius, cm

REFERENCES

1. Cleland, Marshall R.; and Farrell, Paul: Dynamitrons of the Future. IEEE Trans. on Nucl. Sci., vol. 12, no. 3, June 1965, pp. 227-234.

2. Palma, G. E.; and Gagosz, R. M.: Optical Absorption in Fused Silica During Irradiation at High-Temperature. Rep. H-930709-1, United Aircraft Corp. (NASA CR-107838), Nov. 1969.

3. Edwards, Oliver J.: Optical Transmittance of Fused Silica at Elevated Temperatures. J. Opt. Soc. Am., vol. 56, no. 10, Oct. 1966, pp. 1314-1319.

4. Edwards, Oliver J.: Optical Absorption Coefficients of Fused Silica in the Wavelength Range 0.17 to 3.5 Microns From Room Temperature to 980° C. NASA TN D-3257, 1966.

5. Anon.: Corning Fused Silica Code 7940. Data Sheet, Corning Glass Works, 1964.

6. Burrell, Martin O.; Wright, J. J.; and Watts, John W., Jr.: The Calculation of Electron and Brensstrahlung Dose Rates. Protection Against Space Radiation. NASA SP-169, 1968, pp. 529-538.

7. Berger, Martin J.: Transmission and Reflection of Electrons by Aluminum Foils. Rep. Tech. Note 187, National Bureau of Standards, Apr. 1, 1963.

8. Ditchburn, R. W.; Mitchell, E. W. J.; Paige, E. G. S.; Custers, J. F.; Dyer, H. G.; and Clark, C. D.: The Optical Effects of Radiation Damage in Diamond and Quartz. Defects in Crystalline Solids. Univ. of Bristol, 1955, pp. 92-107.

9. van Wieringen, J. S.; and Kats, A.: Paramagnetic Resonance and Optical Investigation of Silicate Glasses and Fused Silica, Coloured by X-Rays. Phillips Res. Rep., vol. 12, 1957, pp. 432-454.

10. Mitchell, E. W. J.; and Paige, E. G. S.: The Optical Effects of Radiation Induced Atomic Damage in Quartz. Phil. Mag., Ser. 8, vol. 1, no. 12, Dec. 1956, pp. 1085-1115.

11. Ruffa, A. R.: Model for the E_1-Center in SiO_2. Phys. Rev. Letters, vol. 25, no. 10, Sept. 7, 1970, pp. 650-652.

12. Nelson, C. M.; and Crawford, J. H., Jr.: Optical Absorption in Irradiated Quartz and Fused Silica. J. Phys. Chem. Solids, vol. 13, 1960, pp. 296-305.

13. Comptom, W. Dale; and Arnold, George W., Jr.: Radiation Effects in Fused Silica and α-Al_2O_3. Disc. Faraday Soc., no. 31, 1961, pp. 130-139.

14. Levy, M.; and Varley, J. H. O.: Radiation Induced Colour Centers in Fused Quartz. Proc. Phys. Soc., Sec. B, vol. 68, pt. 4, Apr. 1955, pp. 223-233.

15. Palma, Gary E.; and Gagosz, Ronald M.: Optical Absorption in Transparent Materials During 1.5 MeV Electron Irradiation. Rep. J-990929-1, United Aircraft Corp. (NASA CR-110907), Oct. 1970.

"The aeronautical and space activities of the United States shall be conducted so as to contribute . . . to the expansion of human knowledge of phenomena in the atmosphere and space. The Administration shall provide for the widest practicable and appropriate dissemination of information concerning its activities and the results thereof."

— NATIONAL AERONAUTICS AND SPACE ACT OF 1958

NASA SCIENTIFIC AND TECHNICAL PUBLICATIONS

TECHNICAL REPORTS: Scientific and technical information considered important, complete, and a lasting contribution to existing knowledge.

TECHNICAL NOTES: Information less broad in scope but nevertheless of importance as a contribution to existing knowledge.

TECHNICAL MEMORANDUMS: Information receiving limited distribution because of preliminary data, security classification, or other reasons.

CONTRACTOR REPORTS: Scientific and technical information generated under a NASA contract or grant and considered an important contribution to existing knowledge.

TECHNICAL TRANSLATIONS: Information published in a foreign language considered to merit NASA distribution in English.

SPECIAL PUBLICATIONS: Information derived from or of value to NASA activities. Publications include conference proceedings, monographs, data compilations, handbooks, sourcebooks, and special bibliographies.

TECHNOLOGY UTILIZATION PUBLICATIONS: Information on technology used by NASA that may be of particular interest in commercial and other non-aerospace applications. Publications include Tech Briefs, Technology Utilization Reports and Technology Surveys.

Details on the availability of these publications may be obtained from:

SCIENTIFIC AND TECHNICAL INFORMATION OFFICE

NATIONAL AERONAUTICS AND SPACE ADMINISTRATION

Washington, D.C. 20546